DETAILED MAPPING OF RESIDENTIAL LAND USE IN QUEZON CITY USING SENTINEL-2 IMAGERY: AN ANALYSIS OF PIXEL-BASED IMAGE CLASSIFICATION USING SUPPORT VECTOR MACHINE

M. I. D. Mabalot[1] *, L. S. Sumera[1] *, A. C. Blanco[1,2], B. G. Carcellar[1]

[1] Department of Geodetic Engineering, University of the Philippines – Diliman, Quezon City, Philippines, (mdmabalot, lssumerajr, acblanco, bgcarcellar)@up.edu.ph
[2] Philippine Space Agency, Diliman, Quezon City, Philippines

Commission IV, WG IV/7

KEY WORDS: Sentinel-2, pixel-based, residential density, SVM, Orfeo Toolbox

ABSTRACT:

Through the years, several studies have attempted to map human settlements using very-high-resolution (VHR) imagery and proprietary software. However, with limitations especially in terms of cost, researchers are now taking the open-source route. For this study, the researchers aimed to perform multi-level classification to delineate residential land use using Sentinel-2 processed with Orfeo Toolbox. The performance of pixel-based approaches with support vector machine (SVM), was applied to different multi-band combinations and varying SVM kernel types. Three sets of information were used – the spectral bands, normalized difference indices, and grey-level co-occurrence matrix (GLCM) measures. In the general land cover classification, except for models with sigmoid kernel, the outputs yielded overall accuracies (OAs) of at least 90%, with special bands and indices raster inputs. The linear kernel performed the best, yielding 93.17% overall accuracy. During the residential versus non-residential built-up cover classification, GLCM measures were added to the set of inputs. The RBF kernel worked best with an OA of 81.56%. The addition of GLCM improved the results, as compared with models with no textural measures. For the residential land use classification, the combination of spectral bands and GLCM, worked best for the pixel-based method, with the linear classifier obtaining the highest OA of 78.24%.

1. INTRODUCTION

One of the popular approaches in settlement mapping is the use of very high-resolution imagery and proprietary applications. While it gives a better understanding of areas, the VHR is costly and inaccessible (Cai et al., 2019). As an alternative, quite a few studies have looked at the potential of medium-resolution imagery, but the usual classification done is up to built-up only. With the advancement of open-source software, studies are now shifting from using commercial to open-source, which now also offers a variety of functions.

The study aimed to develop a pixel-based methodology to map detailed residential land use using medium-resolution imagery and open-source software. Aside from that, the researchers’ specific objectives are to examine the characteristics of land use and land cover based on Sentinel-2; to apply pixel-based classification approaches; to delineate residential land use from the built-up; and to categorize settlements according to density.

With this research, the potential of medium-resolution imagery in human settlement mapping, the feasibility of multi-level classification to categorize built-up covers, and the capability of open-source software in this kind of classification will be explored further. Lastly, the researchers have high hopes that this research will be applied to studies such as disaster risk reduction and management, population, pollution, and public health.

1. STUDY AREA

Quezon City (QC), as shown in Figure 1, is a highly urbanized city that lies in the northeast part of the Metropolitan Manila region in the Philippines. Based on the 2015 Quezon City Ecological Profile, the city is predominantly occupied by

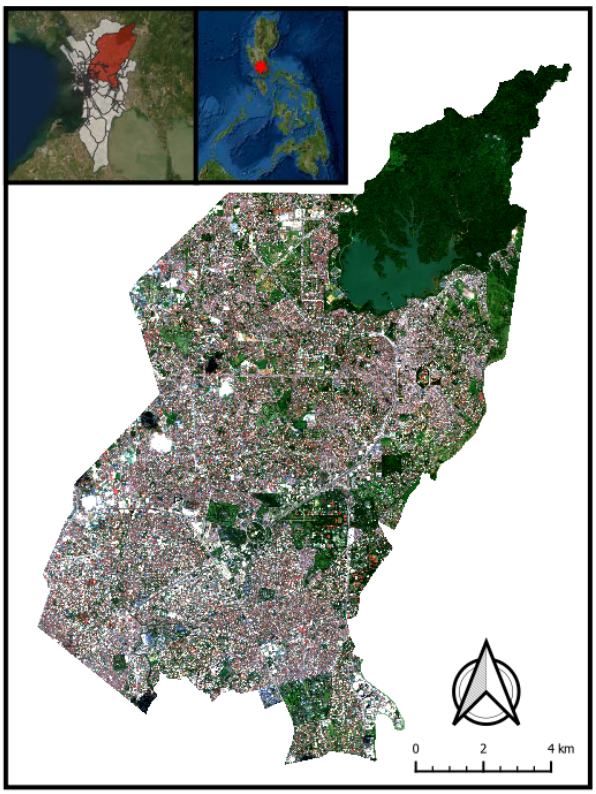

Figure 1. Sentinel-2 true color composite (RGB 432) image covering Quezon City taken on October 25, 2016, with ESRI tile insets showing the Metro Manila area (upper left) and the Philippines (upper center)

residential developments, covering around 41.5% of the land area in 2011. In 2015, 660,249 housing buildings were recorded in the city, the highest in Metro Manila. These were mostly single houses, duplexes, and multi-dwelling complexes (Philippines Statistics Authority, 2017). According to the same report, single housing units have the most number in the city with 332,729, followed by multi-unit residential with 223,917, and duplex with 100,028. The average household size is 4.27, with 4.77 for a single house, 3.66 for multi-unit residential, and 4.03 for a duplex (Philippines Statistics Authority, 2017).

1.1 Quezon City Zoning

The QC's Comprehensive Zoning Ordinance of 2016 categorizes the city's residential areas into three zones: R-1, R-2, and R-3, with some sub-zones: R-1-A and R-2-A, as shown in Table 1.

Residential zone (R-x) /Sub-zone (R-x-x)	Density	Du/ ha*	Density factor	Characteristics
R-1	Low	20	0.0029	Community services and facilities on a neighborhood scale
R-1-A		28	0.0040	
R-2	Medium	60	0.0086	Barangay-level community services and facilities
		45	0.0064	Situated in flood-susceptible areas
R-2-A		100	0.014	Community services and facilities at outlying barangay scale
		80	0.011	Situated in flood-susceptible areas
R-3	High	>101	Varies	More than usual services and facilities Caters more distant areas
		115	0.016	Situated in flood-susceptible areas

* du/ha = dwelling units per hectare

Table 1. Residential Zone/Subzone Classification (Quezon City Government, 2016)

To get the density factor, the equation below was used (Quezon City Government, 2016):

$$u = L \times df \quad (1)$$

where: u = number of dwelling units allowed
L = area in square meters less open space requirements
df = density factor

Another dwelling area identified is the Socialized Housing Zone (SHZ). In Quezon City, uses allowed in the residential zones are also permitted in a socialized housing zone (Quezon City Government, 2016).

1.2 Limitation

For the Level 1 or general land cover classification, golf courses, cemeteries, water utilities, and other similar features were not considered. These will confuse the classifier and are likely to be misclassified. As for Levels 2 and 3 (residential vs. non-residential built-up cover and residential land use respectively), condominiums and multi-household buildings, as well as mixed-use infrastructures, were excluded from the analysis. These infrastructures have multiple functions and by observing satellite imagery, their appearances are more similar to non-residential built-up areas. With the exclusion of vertical developments, the study was able to categorize conventional dwelling units.

2. METHODOLOGY

2.1 Data Used

Optical data such as satellite imagery were collected to perform processing and validation. Polygon and line shapefiles were also acquired to aid the selection of samples and ground truths. As additional references to clearly see the details of the study area, tile maps were also used. Listed in Table 2 are all the data acquired and used for the study.

2.2 Applications Used

In this study, the researchers utilized QGIS (3.16.16-Hannover), an open-source geographic information system. Aside from this, the GDAL (3.4.1), a library used for geospatial operations (GDAL/OG Contributors, 2022), was installed. For the pre-processing, the SNAP (Sentinel Application Platform) Desktop (8.0.9) was used with the Sen2Cor255 plugin. To perform the classification, the Orfeo Toolbox (OTB) (7.4.0) was employed through QGIS. OTB is an open-source software library used in processing remote sensing products (OTB Team, 2021).

Data	Type	Source
Sentinel-2 L1C Data Sensing acquisition date: 2016-10-25, 02:17:52	Satellite Image	Copernicus Open Access Hub (https://scihub.copernicus.eu/)
Planet Imagery Sensing acquisition date: 2016-11-20, 01:38:40; 2016-11-20, 01:38:41; 2016-11-20, 01:38:42;		Planet Labs
QC Political Boundary	Polygon	Quezon City Planning and Development Department
2009 QC Land Use Map		
2016 QC Zoning Map		
QC Road Network	Line	
QC Waterways		
Greater Metro Manila Area Exposure Database	Polygon	Philippine Institute of Volcanology and Seismology
2003 Metropolitan Manila Earthquake Impact Reduction Study (MMEIRS) Land Use Map		Geoportal Philippines (https://www.geoportal.gov.ph/)
OpenStreetMap	XYZ Tile	OpenStreetMap (https://tile.openstreetmap.org/{z}/{x}/{y}.png)
ESRI Imagery		ArcGIS Online (https://server.arcgisonline.com/ArcGIS/rest/services/World_Imagery/MapServer/tile/{z}/{y}/{x})

Table 2: Data acquired and used in mapping residential land use of different densities in Quezon City, Philippines

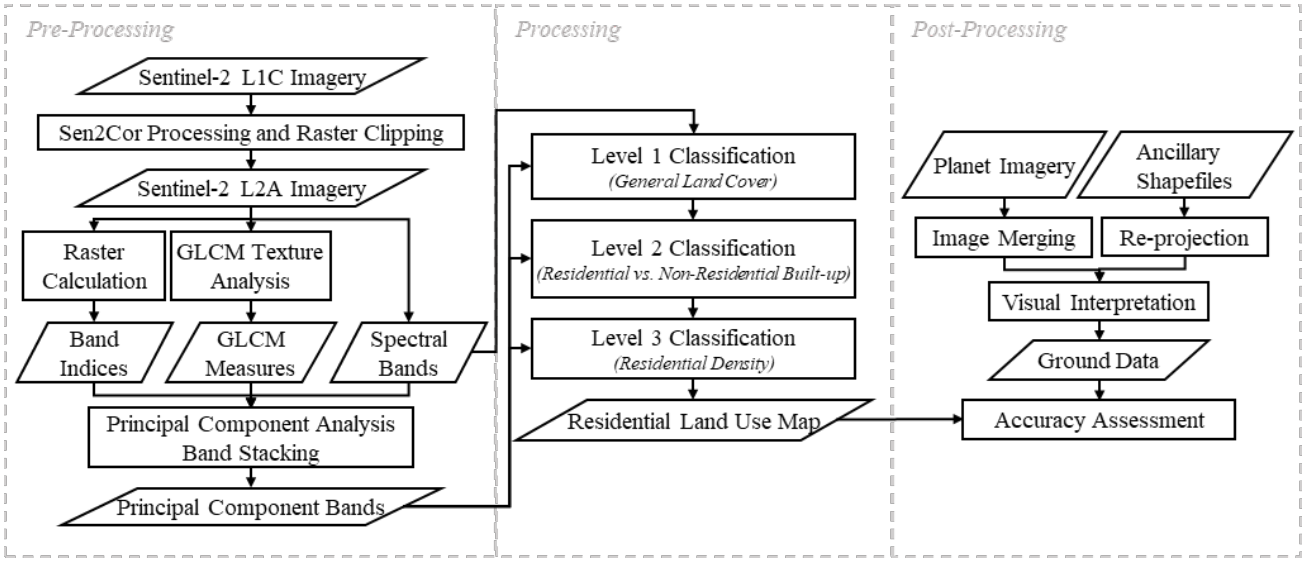

Figure 2. General workflow of the study. Classification of the image data set is carried out using Support Vector Machine.

2.3 General Workflow

The workflow was divided into three main parts: pre-processing, processing, and post-processing, as shown in Figure 2. The pre-processing comprised data preparation, extraction, and principal component analysis. During the processing stage, the pixel-based image classification using a support vector machine (SVM) classifier was implemented. A multi-level classification was also conducted, from broad to a more detailed classification. Lastly, the post-processing involved accuracy assessment and validation. These will be discussed further in the next sections.

2.4 Pre-Processing

2.4.1 Sentinel-2 Imagery L2A Generation

The Sentinel-2 Level 2A products can be generated from the user side by feeding an L1C product into the Sentinel-2 Toolbox in which corrections are done to generate bottom-of-atmosphere reflectance (European Space Agency, 2015). The resulting product consists of the following bands shown in Table 3.

	Band	Central Wavelength (nm)	Spatial Resolution (m)
1	Coastal aerosol	443	60
2	Blue	490	10
3	Green	560	10
4	Red	665	10
5	Vegetation red edge	705	20
6		740	20
7		783	20
8	Near-infrared (NIR)	842	10
8a	Narrow near-infrared	865	20
9	Water vapor	945	60
11	Shortwave Infrared (SWIR)	1610	20
12		2190	20

Table 3. Sentinel-2 Spectral Bands and Resolution (European Space Agency, 2015)

2.4.2 Information Extraction

Three types of information were extracted: spectral bands, normalized difference indices, and gray-level co-occurrence matrix (GLCM) textural measures.

2.4.2.1 Normalized Difference Indices

Commonly used band indices were extracted: the normalized difference vegetation index (NDVI), the normalized difference water index (NDWI), and the normalized difference built-up index (NDBI). The following equations calculate these indices:

$$NDVI = \frac{(NIR - Red)}{(NIR + Red)} \quad \text{(Kriegler et al., 1969)} \quad (2)$$

$$NDWI = \frac{(Green - NIR)}{(Green + NIR)} \quad \text{(McFeeters, 1996)} \quad (3)$$

$$NDBI = \frac{(SWIR - NIR)}{(SWIR + NIR)} \quad \text{(Zha, Gao \& Ni, 2003)} \quad (4)$$

2.4.2.2 Gray-Level Co-Occurrence Matrix (GLCM)

According to Hall-Beyer (2017), the GLCM approach is a technique for obtaining second-order statistical texture features, determined by measuring the relationship of a neighborhood using displacement, directionality, and gray limits. Equations 5 to 14 (Hall-Beyer, 2017) describe the textural measures used.

The Sentinel-2 bands blue (B02), green (B03), red (B04), and NIR (B08) were used to produce GLCM features. The following window sizes were evaluated to examine the effect of the kernel size on the built-up cover classification: 5x5, 7x7, 9x9, and 11x11. A total of 40 outputs per window size were generated, with each 10-m band having ten (10) textural measures.

Measure	Equation	
Contrast	$\text{Contrast} = \sum_{i,j=0}^{N-1} P_{i,j}(i-j)^2$	(5)

Dissimilarity	$\text{Dissimilarity} = \sum_{i,j=0}^{N-1} P_{i,j}\lvert i-j\rvert$	(6)
Homogeneity	$\text{Homogeneity} = \sum_{i,j=0}^{N-1} \frac{P_{i,j}}{1+(i-j)^2}$	(7)
Angular Second Moment	$\text{ASM} = \sum_{i,j=0}^{N-1} P_{i,j}^2$	(8)
Energy	$\text{Energy} = \sqrt{\text{ASM}}$	(9)
Maximum Probability	$\text{Maximum Probability} = \max(P_{i,j})$	(10)
Entropy	$\text{Entropy} = \sum_{i,j=0}^{N-1} P_{i,j}(-\ln P_{i,j})$	(11)
GLCM Mean	$\mu_i = \sum_{i,j=0}^{N-1} i(P_{i,j}) \quad \mu_j = \sum_{i,j=0}^{N-1} j(P_{i,j})$	(12)
GLCM Variance	$\sigma_i^2 = \sum_{i,j=0}^{N-1} P_{i,j}(i-\mu_i)^2$ $\sigma_j^2 = \sum_{i,j=0}^{N-1} P_{i,j}(j-\mu_j)^2$	(13)
Correlation	$\text{Correlation} = \sum_{i,j=0}^{N-1} P_{i,j}\left[\frac{(i-\mu_i)(i-\mu_j)}{\sqrt{(\sigma_i^2)(\sigma_j^2)}}\right]$	(14)

Table 4. GLCM textural measures used for the study

2.4.3 Principal Component Analysis

The Principal Component Analysis (PCA) orthogonally transforms input bands into rotated axes, reducing redundancy and noise (Rana & Venkata Suryanarayana, 2020). To reduce the dimensionality of the information, PCA was performed on the spectral bands, band indices, and GLCM measures generated.

2.4.4 Raster Inputs

After getting the principal components, band stacking was done to create combinations of information. Tabulated in Table 5 are the combinations of raster inputs used for each level.

Level	Information	GLCM window size	Total raster input
1	Original spectral bands Band indices	-	2
	PC band indices PC spectral bands		
2 and 3	PC band indices PC spectral bands	5x5 7x7 9x9 11x11	13
	PC band indices PC GLCM		
	PC spectral bands PC GLCM		
	PC band indices PC spectral bands PC GLCM		

Table 5. Image combination of the raster inputs per level

2.5 Processing

2.5.1 Training and Validation Data

To create training data, the visual characteristics of each feature were observed by comparing the Sentinel-2 imagery with the collected land use and zoning maps, road network, and OSM. For unclear areas, the ESRI tile map was viewed instead. The initial samples created were polygons. From these data, random data, random and periodic point data were derived.

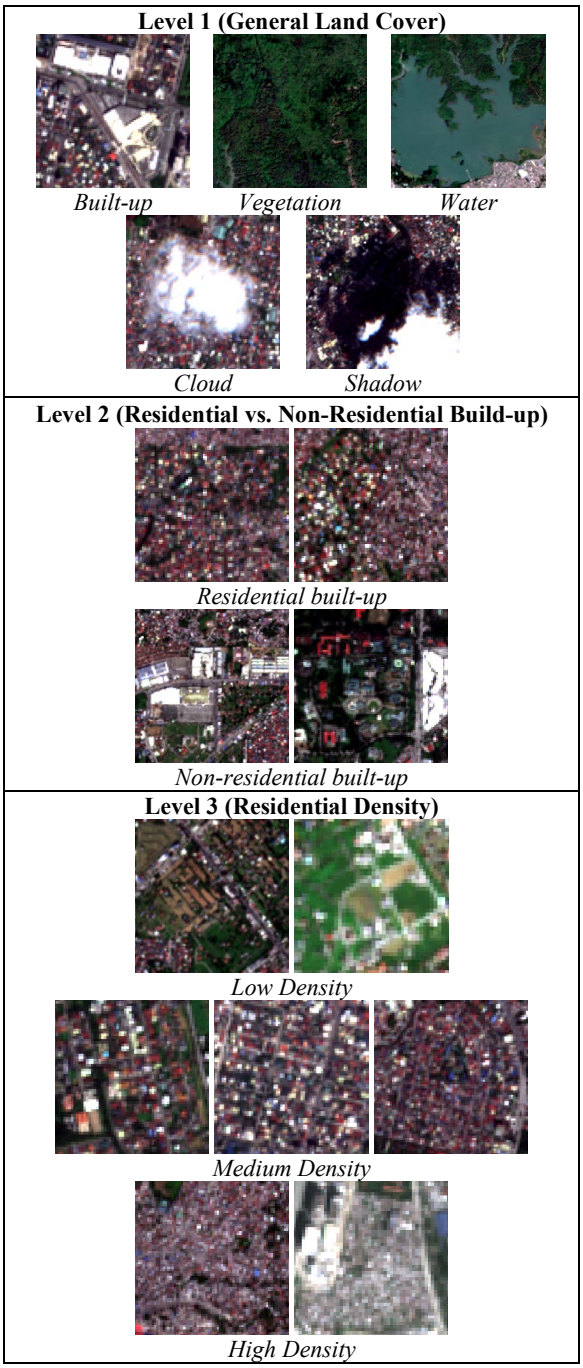

Figure 3. Sample Sentinel-2 image subsets for each land use land cover class in different levels of classification

Five (5) classes were identified in Level 1 or the general land cover processing: built-up, vegetation, water, cloud, and shadow. Level 2 focused on the classification of built-up cover, by separating the residential and the non-residential cover. Elements analyzed in categorizing the built-up cover were color, shape, size pattern, and association. The location and presence of shadows were also examined to delineate non-residential cover.

In classifying the residential built-up according to density, three (3) classes were determined: low, medium, and high. This division was according to the spaces of the houses, organization/ pattern, and the zoning classification they belong to. Shown in Figure 3 are the Sentinel-2 image samples of each class.

For the validation set, ground truths were taken from the land use and zoning map for Levels 1 and 2. Calculations using Eq. 1 and visual interpretation were done to get Level 3 validation data.

2.5.2 Pixel-Based Image Classification

Figure 4 describes the workflow of the supervised pixel-based image classification performed on the Orfeo Toolbox (OTB Team, 2018), excluding the sieve analysis.

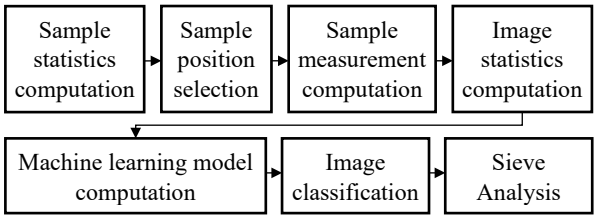

Figure 4. Pixel-based image classification workflow

As an additional analysis to improve the appearance of the outputs, sieving was performed. The function omits clusters of pixels that have sizes below the threshold value and then replaces them with a pixel value of a much larger neighboring pixel value (GDAL/OGR Contributors, 2022). Various sieve threshold values, t, were explored.

2.5.3 Classification with Support Vector Machine

The image classification was employed with support vector machine (SVM), a machine learning algorithm. According to Wieland and Pittore (2016), it is believed to be the most suitable technique for studying built-up and urban structure types. The goal of SVM is to identify a hyperplane with the widest margin.

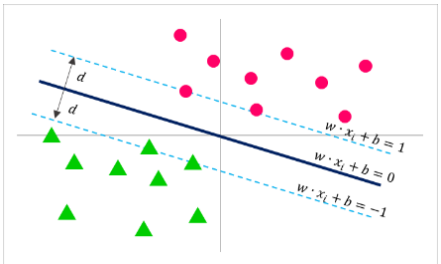

Figure 5: Illustration of the Linear SVM algorithm

Figure 5 visualizes the SVM. For each vector, x_i, the hyperplane is defined (Berwick, 2011):

$$w \cdot x_i + b \geq 1 \text{ for } x_i \text{ when } y_i = 1 \quad (15)$$

or

$$w \cdot x_i + b \leq -1 \text{ for } x_i \text{ when } y_i = -1 \quad (16)$$

As explained by Berwick (2011), if the equation of the plane, $w \cdot x_i + b = 0$ is satisfied, the decision boundary is obtained. If the equation $w \cdot x_i + b = 1$ is satisfied, a positive (+) class plane is obtained for all positive x points that satisfy Equation 15. On the other hand, if $w \cdot x_i + b = -1$ is satisfied, a negative (-) class plane is obtained for all negative x points that satisfy the Equation 16.

Aside from linear, three (3) other kernel types were explored: polynomial, radial basis function (RBF), and sigmoid. These are expressed as follows (Hsu, Chang & Lin, 2003):

$$\text{Linear} \quad K(x_i, x_j) = x_i^T x_j \quad (17)$$

$$\text{Polynomial} \quad K(x_i, x_j) = (\gamma x_i^T x_j + r)^d, \ \gamma > 0 \quad (18)$$

$$\text{Radial basis function} \quad K(x_i, x_j) = \exp\left(-\gamma \|x_i - x_j\|^2\right), \ \gamma > 0 \quad (19)$$

$$\text{Sigmoid} \quad K(x_i, x_j) = \tanh(\gamma x_i^T x_j + r) \quad (20)$$

2.5.4 Multi-Level Classification

According to Sideris and co-authors, the Orfeo toolbox cannot straightforwardly perform multi-level classification. However, a workaround is by re-processing the image and masking out portions not requiring any further classification and merging the results with the previous output. With this, for each level of classification, different sets of sieving threshold values were used in an attempt to improve the data. Different kernel types and raster inputs were also tried.

2.6 Post-Processing

Using the validation features created earlier, the accuracy assessment was carried out by generating confusion matrices and determining the kappa coefficient. Visual analysis was also done to compare the outputs generated and examine the results and determine which parts were misclassified. This also allowed the researchers to improve the classification accuracy.

3. RESULTS AND DISCUSSIONS

3.1 Principal Component Analysis (PCA)

As discussed earlier, PCA was performed to reduce the dimensionality of the spectral bands, indices, and GLCM measures. For the study, 95% of the data variation was retained. Tabulated in Table 6 are the cumulative variances and the number of principal components used as part of the raster inputs.

Information	Cumulative Variance (%)	Original Number of Bands	Number of Principal Components Retained
Spectral bands	97.459	12	3
Band indices	99.330	3	2
GLCM (5x5)	95.246	40	9
GLCM (7x7)	95.032	40	8
GLCM (9x9)	95.544	40	8
GLCM (11x11)	95.855	40	8

Table 6. Principal component analysis results of the information extracted

Shown in Figure 6 are the single-band renders of some of the first principal components (PC) extracted. Looking at the first PCs of spectral bands and indices, the two looked alike, putting emphasis particularly on large built-up structures as well as clouds. While grain the GLCM (5x5)'s component band was crisper than 11x11 which was quite blurry.

3.2 Level 1 Classification (General Land Use)

Shown in Figure 7 are the kappa indices and the overall accuracies of Level 1 models. An insignificant difference was

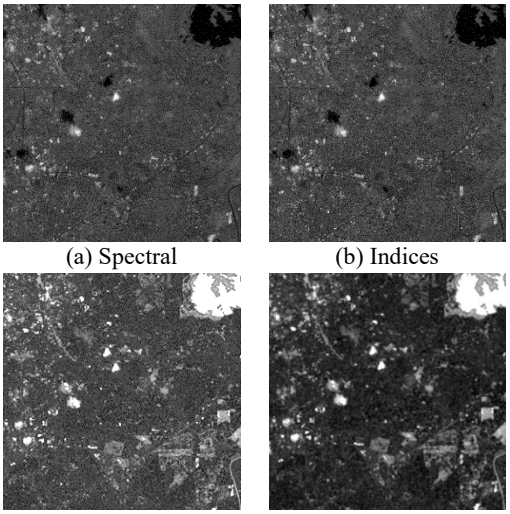

(a) Spectral (b) Indices

(c) GLCM (5x5) (d) GLCM (11x11)

Figure 6. Single-band gray renders of the first principal component bands extracted using (a) Spectral bands, (b) Indices derived from the Spectral band, (c) GLCM (5x5) layers, and (d) GLCM (11x11) layers.

seen with the use of random and periodic sampling types. The linear, RBF, and polynomial kernel produced good results with an overall accuracy of at least 90%. In terms of kappa indices, the models which scored at least 0.81 translated to almost perfect strength of agreement (Landis and Koch, 1977) while the rest except for the sigmoid models achieved substantial strength of agreement. Comparing the kernel types, linear worked best with the original spectral bands and indices input. RBF and polynomial were more effective when using PC bands. Among the outputs, the linear random model with the original band set achieved the highest OA.

As discussed earlier, sieving was done to remove grain-like pixels on the output images. By performing this, the researchers were also able to check whether sieving improves the classification not just visually, but also numerically. Figure 8 shows a reference satellite image and the comparison of the original (un-sieved) output with the sieved images of the linear random model with the original band set. As the threshold parameter is increased, more speckles are removed. However, relatively bigger clusters of pixels are more likely to be omitted too. While sieving visually enhanced the output images, slightly lower scores were achieved by the original band set models. For the principal component models, most of the output benefitted from it, except for the linear random model.

Of all the outputs it can be noted that the sigmoid kernel performed poorly. With this, the outputs were disregarded and for the next levels, the testing was discontinued.

Tabulated in Table 7 are the best overall accuracies of the models. The high overall accuracy of the linear, RBF, and polynomial kernels indicates that the data can be separated not only linearly but can also be isolated using non-linear means.

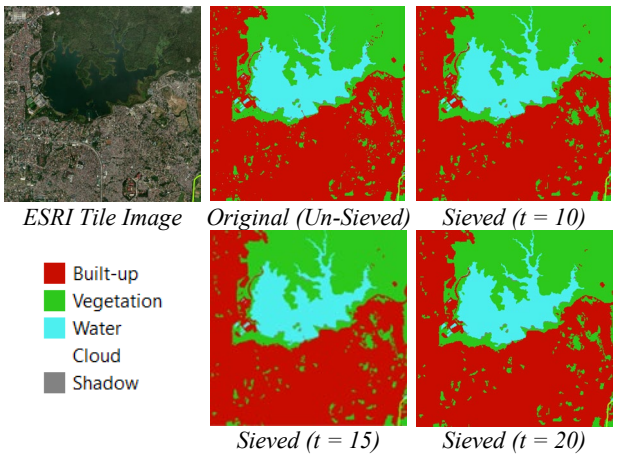

Figure 8. Original and sieved outputs (Level 1 best output)

Input Raster	Kernel	Sampling type, Sieve threshold	OA (%)
Original	Linear	Random, original	93.17
	RBF		90.38
	Polynomial		92.05
PC	Linear		90.80
	RBF	Periodic, t = 10	93.17
	Polynomial	Periodic, t = 20	93.17

Table 7. Top-performing Level 1 outputs (per kernel type)

Shown in Figure 9 is the best-performing output. Visually, the output was a little bit grainy, a manifestation of salt-and-pepper effect. Despite this, the water feature (river) can still be seen.

3.3 Level 2 Classification (Residential vs. Non-Residential

Similar to Level 1, the sampling type (random or periodic) to use does not really matter as the performances of each model are almost the same with their counterpart. To simplify, the next figure (Figure 10) will describe the models with random samples.

Generalizing the trends, the OA increase as the window size of the GLCM widens. Moreover, with the absence of GLCM bands, the OA drops significantly. In terms of raster input composition,

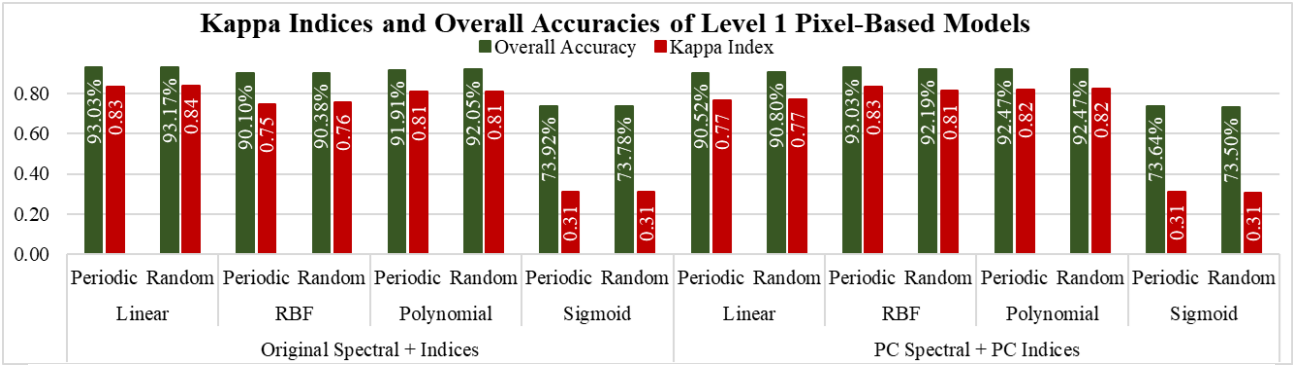

Figure 7. Kappa Indices and OAs of Level 1 Models

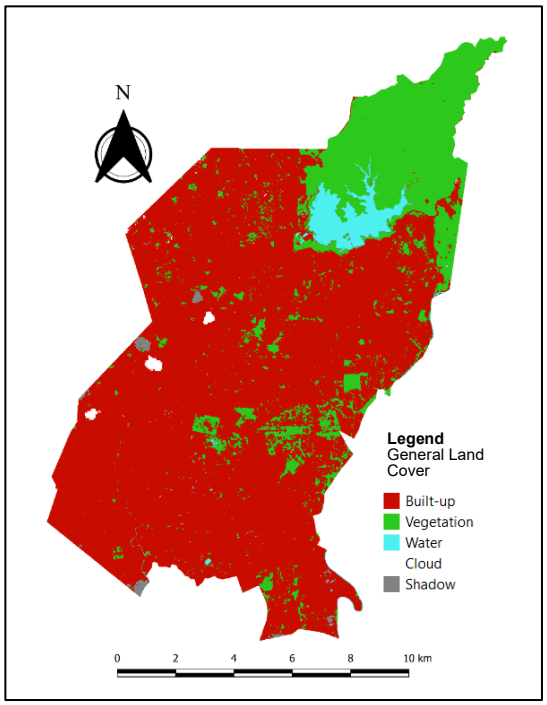

Figure 9. Best-performing Level 1 output (93.17% OA)

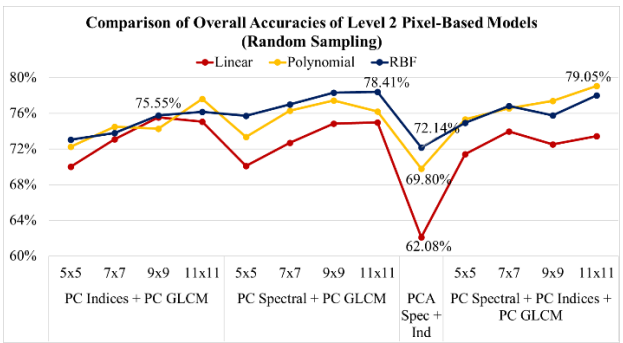

Figure 10. Overall accuracies of the Level 2 random models

on average, both the linear and polynomial kernels achieved good outputs with PC spectral and PC GLCM input. The linear kernel had a better set of results with PC indices and PC GLCM raster. For the pixel-based approach, the random polynomial model with raster input PC spectral, PC indices, and PC GLCM (11x11) achieved the highest OA, with 83.25%. With these results, it is recommended to use PC spectral and PC GLCM raster input for the Level 2 classification. The use of textural measures such as GLCM improves built-up extraction as the models without GLCM measure gave significantly lower scores.

In terms of overall accuracies per kernel type, polynomial achieved the best set of results, closely followed by RBF. The linear models yielded the lowest set of performances, indicating that the data were not linearly separable data, thus, the non-linear kernel worked better. Based on Landis and Koch's (1977) scale, all the scores obtained exhibit moderate strength of agreement.

Figure 11 shows the sieving results for the top-performing pixel-based output. An increase in OAs was also seen in the sieved outputs compared with the original. Threshold value 25 was more fit with the linear and polynomial models. For the RBF kernel, improvement was significant with t = 30. With this, it is important to determine the most optimal threshold value for a given kernel type.

Tabulated in Table 8 are the overall accuracies of the top-performing models.

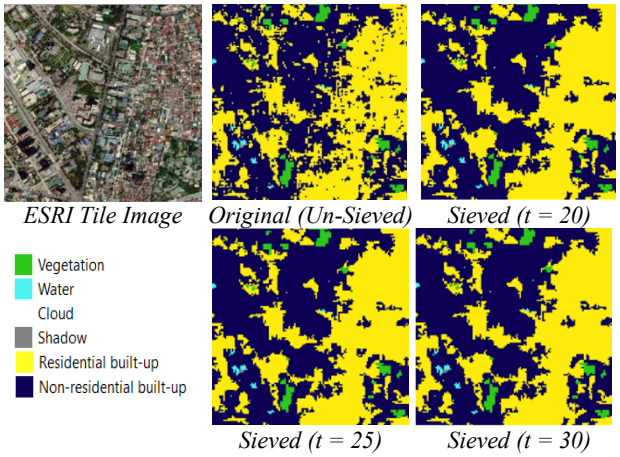

Figure 11. Original and sieved outputs (Level 2 best output)

Kernel	Input raster, Sieve threshold	OA (%)
Linear	PC indices + PC GLCM (9x9), t = 30	76.17
Polynomial	PC spectral + PC indices + PC GLCM (11x11), t = 25	81.56
RBF	PC spectral + PC GLCM (11x11), t = 25	80.29

Table 8. Top-performing Level 2 outputs

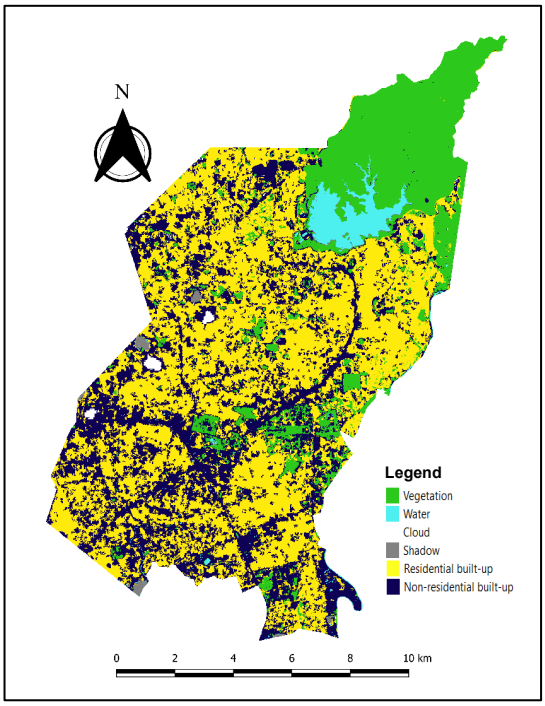

Figure 12. Best-performing Level 2 output (81.56% OA) showing land use land cover in Quezon City, with two classes of built-up areas: residential and non-residential.

Figure 12 shows the top-performing models for Level 2. The salt-and-pepper effect was less exhibited since sieving removed the grains around the original output.

3.4 Level 3 (Residential Land Use According to Density)

Moving forward to the Level 3 classification, unsurprisingly, the results of both the periodic and random sampling were

comparable. But for simplicity, the next figures will show the results of the models which used random samples.

Figure 13 presents the overall accuracies of the Level 3 models (random sampling). For all the kernel types, particularly the models with PC indices and PC GLCM input, the OA increased as the GLCM window enlarges. This trend is also followed by the polynomial models with PC spectral, PC indices, and PC GLCM raster. For the RBF and polynomial models with input PC spectral and PC GLCM, the OA peaked at 9x9. For the rest of the image inputs of the linear classifier, the performance climaxed at a 7x7 window size. Focusing on the raster input, the linear and polynomial models worked well with PC spectral and PC GLCM combination. The RBF kernel, meanwhile, got better results with PC indices and PC GLCM band set. Moreover, RBF should not be mixed with PC spectral, PC indices, and PC GLCM as it yields the lowest set of results. For the Level 3 pixel-based approach, the random linear model with PC spectral and PC GLCM (9x9) scored the highest OA. The polynomial and RBF models’ best performing outputs also used the same raster inputs.

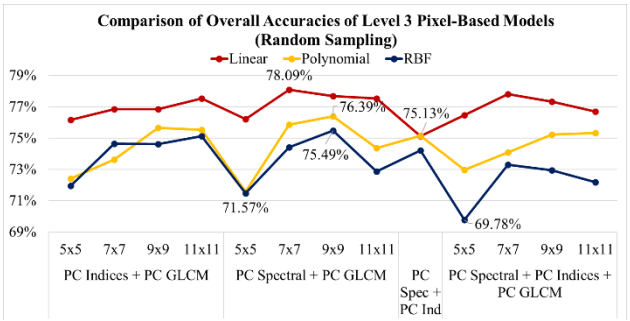

Figure 13: Overall accuracies of the Level 3 random models

In terms of the median kappa index per kernel type, the linear models obtained the highest median kappa index of 0.5857. the polynomial and RBF classifiers attained scores of 0.5503 and 0.5130, respectively. All of them translate to moderate strength of agreement, based on the scale of Landis and Koch (1977). Similarly, the linear model got the highest median overall accuracy, followed by polynomial, and lastly, RBF.

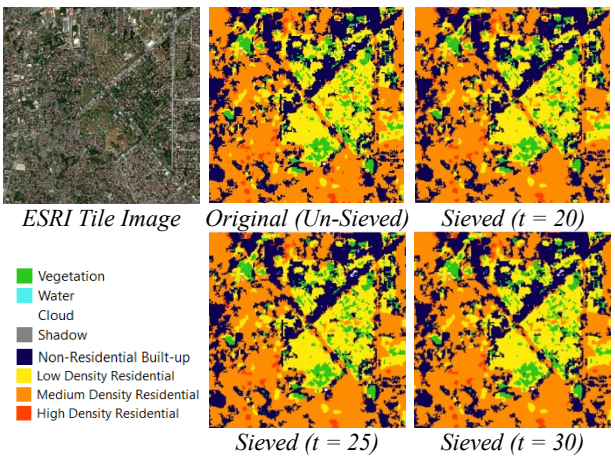

Figure 14. Original and sieved outputs (Level 3 best output)

Sieving was once again performed, as shown in Figure 14. Same with Level 2, the overall accuracies improve as the threshold increases. Moreover, the linear and polynomial models were enhanced as the sieve threshold increased. Small refinement was seen in the RBF models. Overall, while there is an improvement, these were very minimal.

Listed in Table 9 are the top-performing models for Level 3.

Kernel	Input raster, Sieve threshold	OA (%)
Linear	PC spectral + PC GLCM (7x7), t = 30	78.24
Polynomial	PC spectral + PC GLCM (9x9), t = 25	76.56
RBF	PC spectral + PC GLCM (9x9), t = 30	77.34

Table 9. Top-performing Level 3 outputs

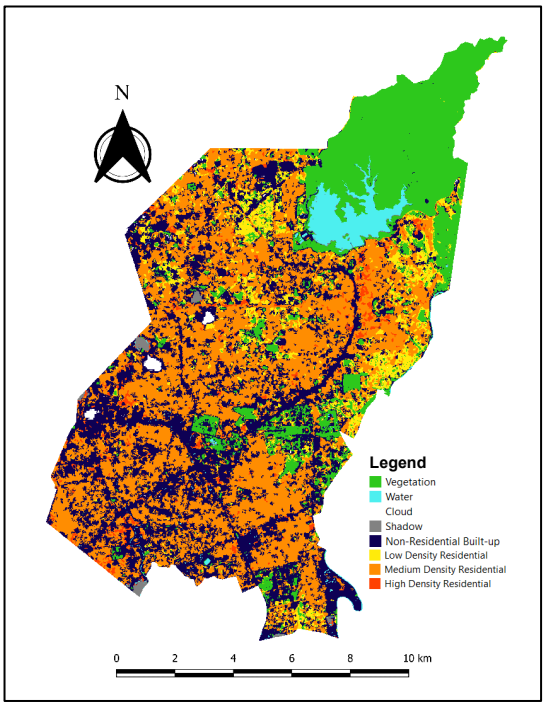

Figure 15. Best-performing Level 3 output (78.14% OA) showing land use land cover in Quezon City, including residential areas of various densities.

Looking at the top-performing output shown in Figure 15, most of the residential built-ups were classified as medium density. The output was able to correctly capture the areas predominantly filled with low-density settlements. While the model was able to identify the low, medium, and high-density residential areas, there was a quite mismatch with the definition of the residential zone if the Philippine zoning classification scheme was followed. The classified low-density settlements only included sparse houses. The high density covered cramped communities, particularly informal settlements. Meanwhile, the medium-density class included low-density but adjacent housing communities, medium zones, and organized high-density areas. Moreover, based on the outputs, some informal settlements were classified as medium, instead of high. The researchers believe that larger training samples, both in number and in polygon size, can improve the results. With bigger polygon training samples, the classifier will be able to get to know the overall characteristics of each residential type. It is critical to include not only the houses representing each class but also the surrounding environment for the classifier to learn about the environment. With more samples, the misclassified areas will be lessened.

Comparing the OA and kappa indices of Level 3 to the preceding levels, this level produced the lowest results. As the classification becomes more detailed, the performance of the models degrades. Because the optical data processed was only of medium resolution, the information provided by the Sentinel-2 imagery might not be adequate to cover the data needed to accurately delineate residential density. To improve the results, it is

recommended to explore other data that will better capture the built-up densities. Despite Sentinel-2 being a medium-resolution imagery, with its performances during Levels 1, 2, and 3, it has good potential in classifying residential density.

4. CONCLUSION

In this study, the researchers conducted pixel-based image classification to map the residential land use in Quezon City. For the Level 1 (general land cover) classification, the linear kernel yielded the best result. At Level 2 (residential vs. non-residential built-up), the presence of GLCM measures significantly improved the classification. With exception of a few models, as the GLCM window size increase, the model performance improves. The polynomial kernel was the most optimal kernel. Finally, for the Level 3 (residential land use) classification, the models with linear kernel obtained the highest overall accuracies with linear kernel type. Moreover, the absence of band indices in the raster images produced outputs with higher overall accuracies. With these results, the research was able to classify general land cover, delineate the residential cover from the built-up cover, and categorize the human settlements according to their residential density using pixel-based image classification with SVM. Despite the limitations of the data used, it was able to map the residential density with 78.24% overall accuracy.

4.1 RECOMMENDATION

To overcome the salt-and-pepper effects, researchers should test more threshold values to determine the number that not only removes most grains but also numerically enhances the results. Other post-processing techniques besides sieve and clump analysis must also be explored.

In general, more samples should be added to areas where misclassification occurred to improve the results. Larger coverage of training polygon is also recommended to provide additional context. In terms of data, aside from optical data, other types like synthetic aperture radar and point-of-interest data can be explored further. Fieldwork and site visits are strongly recommended. Very high-resolution satellite images such as those in Google Earth can also be used as a quick substitute.

REFERENCES

Berwick, R. (2011). *An Idiot’s Guide to Support vector* [PDF]. Retrieved from Massachusetts Institute of Technology 6.034 Artificial Intelligence Fall Recitations: https://web. mit.edu/ 6.034/wwwbob/

Cai, G., Ren, H., Yang, L., Zhang, N., Du, M., & Wu, C. (2019). Detailed Urban Land Use Land Cover Classification at the Metropolitan Scale Using a Three-Layer Classification Scheme. *Sensors, 19*(14), 3120. doi:10.3390/s19143120

European Space Agency. (2015). *Sentinel-2 User Handbook* [PDF document]. Retrieved from Sentinel Online Document Library: https://sentinels.copernicus.eu/web/sentinel/user-guides/document-library

GDAL/OGR Contributors. (2022). *Geospatial Data Abstraction Library (GDAL) Documentation* [PDF document]. Retrieved April 21, 2022 from GDAL: https://gdal.org/

Hall-Beyer, M. (2017). *GLCM Texture: A Tutorial v. 3.0* [PDF document]. Retrieved from University of Calgary Libraries and Cultural Resources. doi:10.11575/PRISM/33280

Hsu, C., Chang, C., & Lin, C. (2003). *A Practical Guide to Support Vector Classification* [PDF document]. Retrieved from

LIBSVM – A Library for Support Vector Machines: https://www.csie.ntu.edu.tw/~cjlin/libsvm/

Kriegler, F., Malila, W., Nalepka, R., & Richardson, W. (1969). Preprocessing transformations and their effect on multispectral recognition. *Proceedings Of The 6th International Symposium On Remote Sensing Of Environment*, 97-131.

Landis, J., & Koch, G. (1977). The Measurement of Observer Agreement for Categorical Data. *Biometrics, 33*(1), 159. doi:10.2307/2529310

McFeeters, S. K. (1996). The use of the Normalized Difference Water Index (NDWI) in the delineation of open water features. *International Journal of Remote Sensing, 17*(7), 1425–1432. doi:10.1080/01431169608948714

OTB Team. (2021). *Orfeo ToolBox 7.4.1 Documentation*. Retrieved February 8, 2022 from https://www.orfeo-toolbox.org/CookBook-7.4/

QGIS Development Team. (2022). *QGIS Desktop 3.16 User Guide* [PDF document]. Retrieved from QGIS: https://docs. qgis.org/3.16/pdf/en/QGIS-3.16-DesktopUserGuide-en.pdf

Quezon City Government. (2015). *Quezon City Ecological Profile 2015* [PDF document]. Retrieved from QC Profile: https://quezoncity.gov.ph/about-the-city-government/qc-profile/

Quezon City Government. (2016). *Quezon City Comprehensive Zoning Ordinance of 2016 SP-2502, S-2016* [PDF document]. Retrieved from https://quezoncity.gov.ph/wp-content/uploads/ 2021/01/Quezon-City-Zoning-Ordinance-2016.pdf

Rana, V., & Venkata Suryanarayana, T. (2020). Performance evaluation of MLE, RF and SVM classification algorithms for watershed scale land use/land cover mapping using sentinel 2 bands. *Remote Sensing Applications: Society And Environment, 19*. doi:10.1016/j.rsase.2020.100351

Sideris, K., Colson, D., Lightfoot, P., Heeley, L., & Robinson, P. (2020). *Review of image segmentation algorithms for analysing Sentinel-2 data over large geographical areas* (JNCC Report No. 655). Joint Nature Conservation Committee.

Wieland, M., & Pittore, M. (2016). Large-area settlement pattern recognition from landsat-8 data. *ISPRS Journal of Photogrammetry and Remote Sensing, 119*, 294–308. doi:10.1016/j.isprsjprs.2016.06.010

Zha, Y., Gao, J., & Ni, S. (2003). Use of normalized difference built-up index in automatically mapping urban areas from TM imagery. *International Journal of Remote Sensing, 24*(3), 583–594. doi:10.1080/01431160304987